PAPER

Development of CMOS MEMS inductive type tactile sensor with the integration of chrome steel ball force interface

IOP Publishing Journal of Micromechanics and Microengineering
J. Micromech. Microeng. **28** (2018) 044005 (11pp) https://doi.org/10.1088/1361-6439/aaac24

Development of CMOS MEMS inductive type tactile sensor with the integration of chrome steel ball force interface

Sheng-Kai Yeh[1], Heng-Chung Chang[1] and Weileun Fang[1,2]

[1] Power Mechanical Engineering, National Tsing Hua Univ., Hsinchu, Taiwan
[2] Institute of NanoEngineering and MicroSystems, National Tsing Hua Univ., Hsinchu, Taiwan

E-mail: fang@pme.nthu.edu.tw

Received 30 November 2017, revised 14 January 2018
Accepted for publication 31 January 2018
Published 20 February 2018

Abstract

This study presents an inductive tactile sensor with a chrome steel ball sensing interface based on the commercially available standard complementary metal–oxide–semiconductor (CMOS) process (the TSMC 0.18 μm 1P6M CMOS process). The tactile senor has a deformable polymer layer as the spring of the device and no fragile suspended thin film structures are required. As a tactile force is applied on the chrome steel ball, the polymer would deform. The distance between the chrome steel ball and the sensing coil would changed. Thus, the tactile force can be detected by the inductance change of the sensing coil. In short, the chrome steel ball acts as a tactile bump as well as the sensing interface. Experimental results show that the proposed inductive tactile sensor has a sensing range of 0–1.4 N with a sensitivity of 9.22(%/N) and nonlinearity of 2%. Preliminary wireless sensing test is also demonstrated. Moreover, the influence of the process and material issues on the sensor performances have also been investigated.

Keywords: micro tactile sensor, sensing interface, CMOS MEMS

(Some figures may appear in colour only in the online journal)

1. Introduction

Tactile sensors play an important role in various field applications such as the robotics industry, medical devices, consumer products, and so on. To further extend the practical applications of tactile sensors, spatial resolution and the size of the sensing system are critical concerns. In this regard, by using the advantages of the MEMS process, a smaller sensing unit can be realized [1]. Moreover, a tactile force sensing array with much better spatial resolution can also be achieved [2]. Thus, micromachined tactile sensors have been widely reported. Presently, the piezo-resistive and capacitive approaches are two sensing mechanisms frequently being employed for tactile sensors [1–9]. In general, the piezo-resistive sensing approach can be easily affected by thermal noise, while concerns regarding the capacitive sensing technique include the parasitic capacitance and the environmental moisture when the sensing electrodes are exposed to the atmospheric environment. Inductive tactile sensing devices have also attracted a lot of attention recently [10]. They have the potential to achieve wireless transmission of sensing signals according to the characteristics of inductive coupling of two coils.

There are various design concerns for micro tactile sensors. The integration of the micro sensing interface or so called micro tactile bump on the sensing structure is a critical design concern for miniaturized tactile sensors. With a proper sensing interface design, the force can be effectively applied to the tactile sensor. Thus, the design of the sensing interface to solve the contact interface problem has been extensively investigated [1–5]. In addition, many of the micro tactile sensors are consisted of fragile suspended thin film structures. These fragile suspended structures and the attached electrical routines would be damaged as the contact tactile loads exceed the tolerable range. Consequently, the design of suspended structures to survive at a relatively wide loading range are implemented in [2, 9]. These designs could reduce the strain of the sensing part or increase the stiffness of the sensing structure.

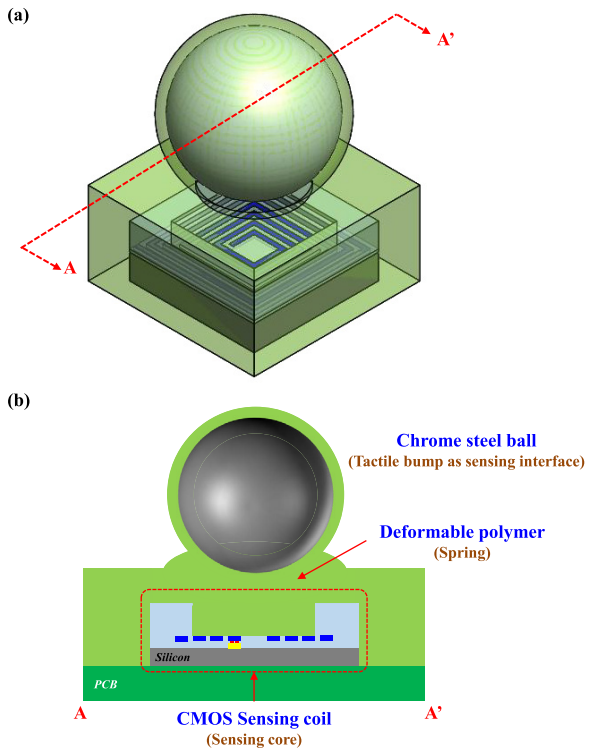

Figure 1. The schematic illustrations of the proposed tactile sensor design consisted of the CMOS sensing coil, polymer filler, and the chrome steel ball sensing interface, (a) a bird's eye view, and (b) the cross-section view.

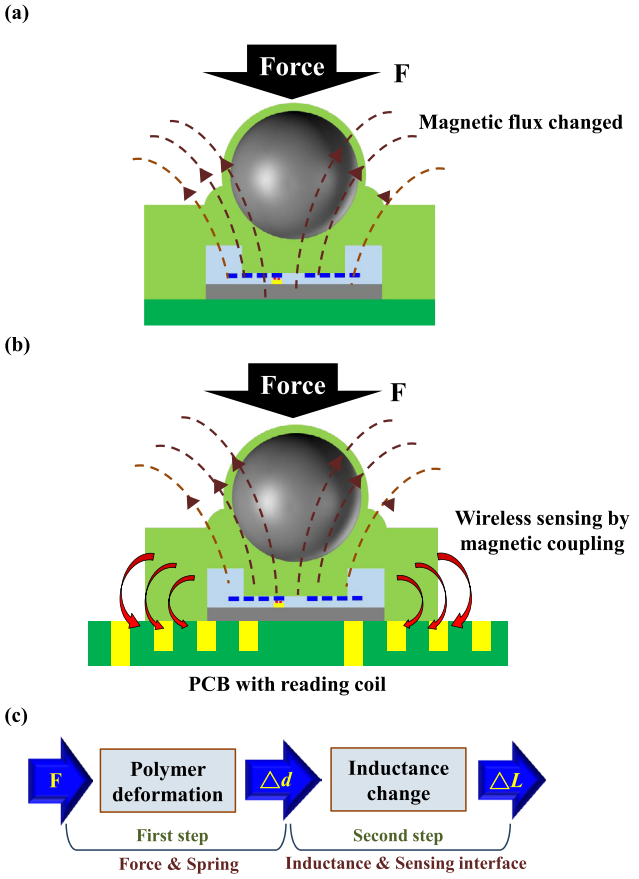

Figure 2. The sensing mechanism of the proposed tactile sensor: (a) a cross-section of AA′ indicates the displacement of chrome steel ball caused by the tactile force will lead the magnetic flux change on sensing coil, (b) the passive wireless sensing mechanism using the PCB reading coil, and (c) the design schema of the proposed inductive tactile sensor.

This study presents the design of an inductive sensing type tactile sensor, which will integrate with a chrome steel ball as the tactile bump as well as the sensing interface. The polymer encapsulated on the sensing chip will act as the deformable structure for the tactile load, so that the presented sensor has no fragile suspended thin film structures. Moreover, this study further leverages the mature standard complementary metal–oxide–semiconductor (CMOS) process, which is available in commercial foundries to implement the sensing chip. Compared to the electroplating fabrication process [11–15], the standard CMOS process has the advantages of great electrical routing ability and the possibility of integration with the circuit interface. Thus, it is a promising approach to realize the presented inductive type tactile sensor. As a result, a chip with a sensing coil was designed and implemented based on the Taiwan Semiconductor Manufacture Company (TSMC) 0.18 μm 1P6M standard CMOS process. The standard CMOS process and the post-CMOS sacrificial layer etching process have been exploited in [10] to define the sensing coils and cavity to detect smaller sensing range tactile loads. In this work, additional polymer molding and chrome steel ball assembly processes are exploited to improve the performance of the presented sensor. Moreover, the wireless sensing capability of the presented tactile sensor is also demonstrated.

2. Concept and design

The schematic illustration in figure 1(a) shows the proposed inductive tactile sensor, which consisted of a CMOS chip with a sensing coil and cavity, the molded polymer, and a chrome steel ball. The polymer will filled into the cavity on the CMOS sensing chip and further encapsulated the chip after molding. Moreover, the chrome steel ball was further integrated with the CMOS sensing chip by using the polymer encapsulation. The AA′ cross-section in figure 1(b) indicates the deformable polymer and the rigid chrome steel ball, which act as the spring and the tactile bump, respectively. In addition, the rigid chrome steel ball also acted as the sensing interface. The displacement of the chrome steel ball caused by the tactile force led to the magnetic flux change on sensing coil. Thus, the tactile force could be detected accordingly. Note that the presented tactile sensor had no fragile suspended thin film structures. In addition, the problem resulted from the deformation of the suspended structures (due to the residual stresses and the CTE (coefficient of thermal expansion) mismatch of the thin films for the CMOS chip [16]) is also prevented. Figure 2(a) presents the sensing schema of the inductive type tactile sensor. An AC signal was applied on the sensing coil of the CMOS chip to introduce a magnetic flux. As the force was applied on the rigid chrome steel ball (tactile bump), the flexible polymer (spring) became deformed, and caused the distance to change between the ball and the sensing coil. Hence, the magnetic flux induced by the AC signal was influenced, and changed

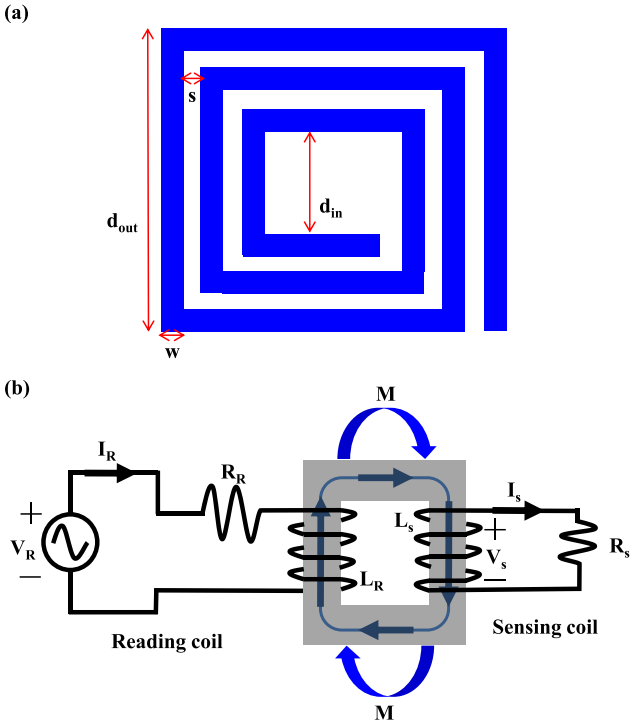

Figure 3. (a) Some important parameters in the rectangular spiral sensing coil, and (b) the equivalent circuit model of the mutual inductance.

the inductance of the sensing coil. Thus, the tactile force was determined by the inductance change of the sensing coil. Moreover, the wireless signal transmission of the presented sensing unit could be achieved by using a reading coil. As indicated in figure 2(b), the reading coil on a separate PCB (printed circuit board) was employed to detect the inductance change of a single sensing unit by using the magnetic coupling effect. For wireless applications, the AC signal was applied only to the reading coil, and the CMOS chip with the sensing coil became a passive device. Note the closed-loop sensing coil was required to enable the magnetic coupling with the reading coil. Figure 2(c) summarizes the design schema of the proposed inductive type tactile sensor.

The planar spiral rectangular coil was employed in this study as the sensing unit. As illustrated in figure 3(a), the spiral sensing coil had an outer length d_{out}, an inner length d_{in}, and the d_{avg} was the average of the inner and outer lengths, $(d_{\text{out}} + d_{\text{in}})/2$. In addition, w was the line width of the coil, s was the interval between the coil, and N was the number of turns of the coil. According to the model in [17], the inductance L (in nano-Henry unit) of the spiral sensing coil in this study can be expressed as,

$$L = \beta d_{out}^{\alpha 1} w^{\alpha 2} d_{avg}^{\alpha 3} N^{\alpha 4} s^{\alpha 5}. \quad (1)$$

The coefficients shown in the above equations are as follows, $\beta = 0.001\,62$, $\{\alpha 1, \alpha 2, \alpha 3, \alpha 4, \alpha 5\} = \{-1.21, -0.147, 2.40, 1.78, -0.03\}$. The planar spiral coils with different shapes are available in [18]. The wireless sensing schema in figure 2(b) can also be predicted from the mutual inductance theory [19]. The schematic equivalent electrical model is depicted in

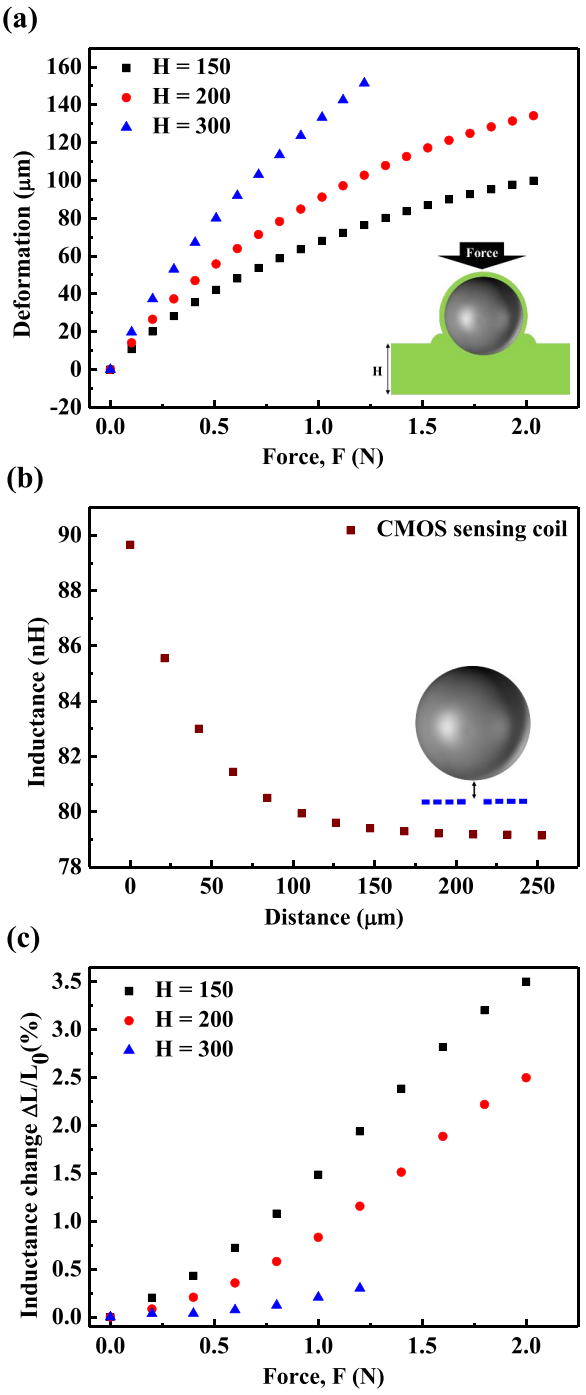

Figure 4. Simulation results: (a) the relation of force and deformation for polymers of different thicknesses, (b) variation of the inductance with the distance between the chrome steel ball and the coil, and (c) the relation of tactile force F and the inductance change $\Delta L/L_0$ for polymer layers of difference thicknesses H.

figure 3(b). The voltage around the sensing loop network (V_s) can be expressed as,

$$V_s = M\frac{dI_R}{dt} - L_s\frac{dI_s}{dt} = I_s R_s \quad (2)$$

where the I_s and L_s are respectively the current and the inductance of the sensing coil, I_R is the current of the reading coil, and M is the mutual inductance between two coils. The mutual

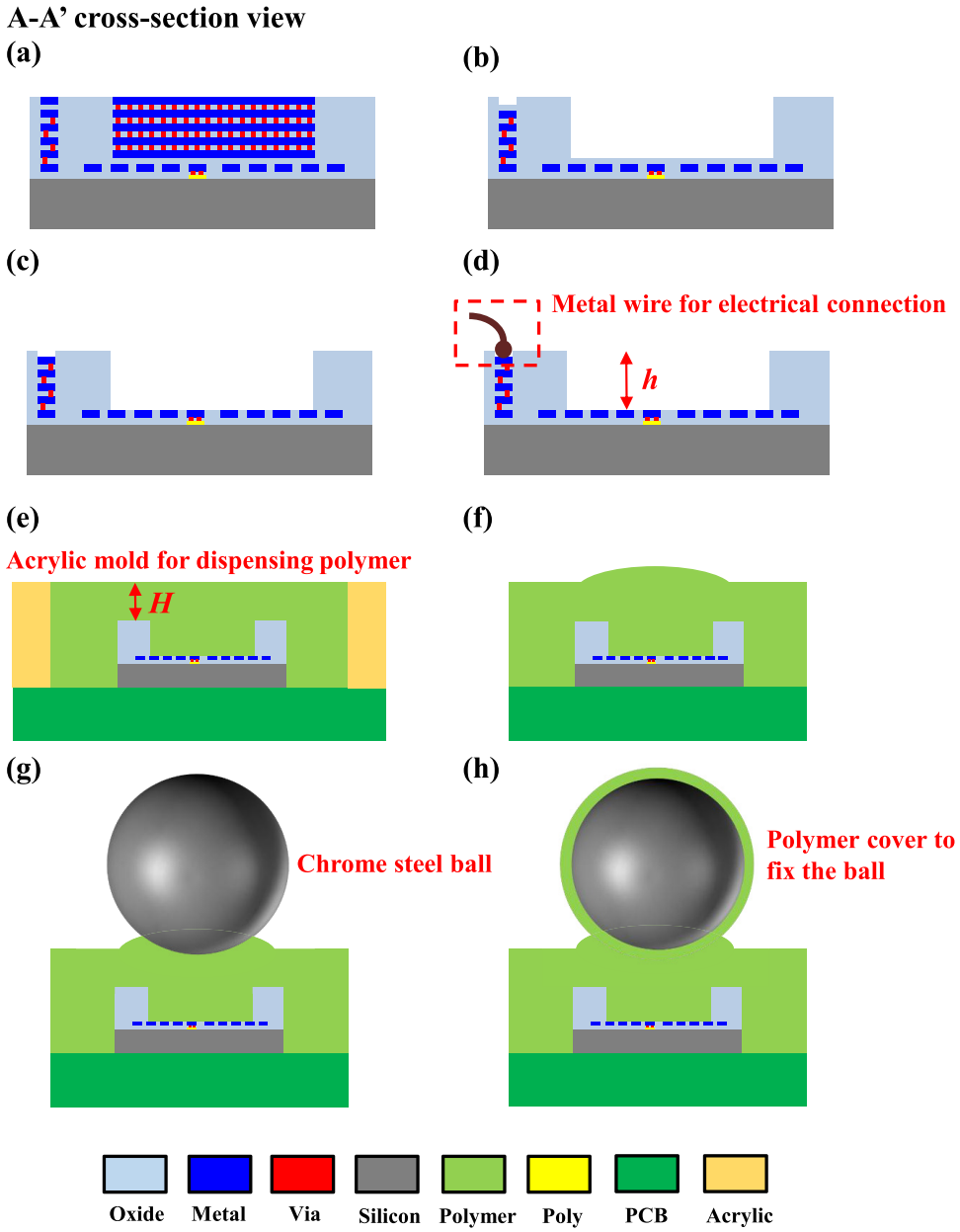

Figure 5. Fabrication processes of the device, (a) CMOS multilayer stacking by the TSMC foundry, (b) metal wet etching to define the thinner cavity, (c) RIE open the bonding pad, (d) wire-bonding for electrical connection, (e) encapsulate the CMOS chip with thicker polymer using the external acrylic molding and cure the polymer, (f) dispense some polymer on the targeted area as the adhesive layer for chrome steel ball, (g) place the chrome steel ball onto the polymer encapsulated chip with the assistant of vacuum head and position stages, and (h) dispense some polymer on the chrome steel ball to fully cover its surface, and cure the polymer to complete the device.

inductance term represents the coupling from the reading coil and acts as the voltage source that drives the sensing part. Moreover, the mutual inductance of the two coils varied with the inductance change of the sensing coil. On the other hand, the voltage around the reading loop network (V_R) can be expressed as,

$$V_R = I_R R_R + L_R \frac{dI_R}{dt} - M\frac{dI_s}{dt} \quad (3)$$

where V_R is the AC voltage source of the reading coil, and L_R is the inductance of the reading coil. Consequently, the variation of mutual inductance M could lead to the inductance change of the reading coil. As a result, the tactile load could be extracted from the inductance change of the reading coils.

In order to verify the design concept of the study, the commercial finite element method (FEM) software (including ANSYS and Ansoft Maxwell) was utilized to predict the performances and characteristics of the proposed device. Following the same gain flow chart introduced in figure 2(c), the hyperelastic model in the ANSYS FEM software was first established to analyze the relationship between the applied force F and the polymer deformation. Figure 4(a) depicts the schematic simulation model with the chrome steel ball and polymer layer of thickness H. The simulation results in figure 4(a) show the deformations of the polymer layers of three different thicknesses ($H = 150$, 200 and 300 μm) when subjected to different applied forces. Note that in the case of $H = 300$ μm, as the force exceeded 1.2 N, the deformation

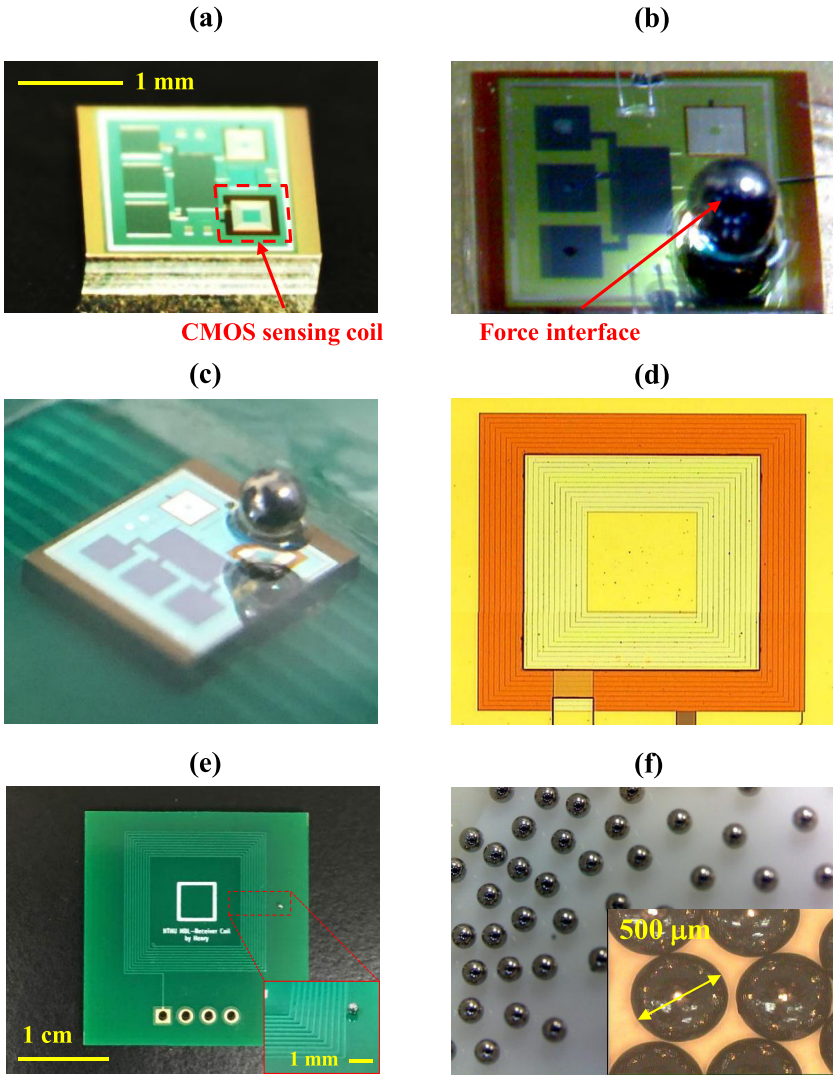

Figure 6. Typical fabrication results of the device, (a) CMOS sensing chip after the etching of sacrificial layers, (b) integration of the polymer encapsulated CMOS sensing chip with the chrome steel ball, (c) the polymer encapsulated sensing chip with chrome steel ball on top of the PCB with reading coil, (d) top view of the CMOS sensing coil, (e) the PCB with reading coil for wireless sensing and the inset show the size difference between the chrome steel ball and the coil, and (f) micrograph of the chrome steel ball.

of the material was too large and the simulation could not converge. According to the simulation results from the Ansoft Maxwell FEM software, figure 4(b) depicts the variation of inductance resulting from the change in distance between the chrome steel ball and the CMOS sensing coil. After the combination of simulations, results in figures 4(a)–(c) further indicate the variation of applied force F and inductance change for the proposed tactile sensors of different thicknesses H. The simulation results show the feasibility of the proposed design. Moreover, the thicker polymer layer H could reduce the stiffness of the sensor and also increase the distance between the chrome steel ball and the sensing coil. As a result, the thicker polymer layer would reduce the sensitivity of the proposed sensor.

3. Fabrication and results

The fabrication processes of the proposed device are presented in figure 5. The proposed tactile sensing chip with coils was implemented by the TSMC 0.18 μm 1P6M standard CMOS process and the in-house post-CMOS micromachining and packaging processes. Firstly, the stacking and patterning of multiple metal and dielectric layers on the chip in figure 5(a) was prepared by the TSMC foundry. Figure 5(b) shows the wet etching process used to remove the metal sacrificial layers by using the H_2SO_4 and H_2O_2 solution [20]. Thus, the cavity on the sensing chip was implemented to provide a space for the application of a small sensing range device [10]. Note that during the metal wet etching process, the sensing coil and electrical routing were protected by the dielectric films. As shown in figure 5(c), the bonding pads were opened by RIE (reactive ion etching) for the following wire-bonding process. As indicated in figure 5(d), the electrical connection was achieved after the wire-bonding of electrical pads. As illustrated in figure 5(e), the polymer molding was implemented with the assistance of the acrylic mold, and the sensing chip was then encapsulated. The volume of the polymer was controlled by a commercial pneumatic polymer dispensing system. In addition

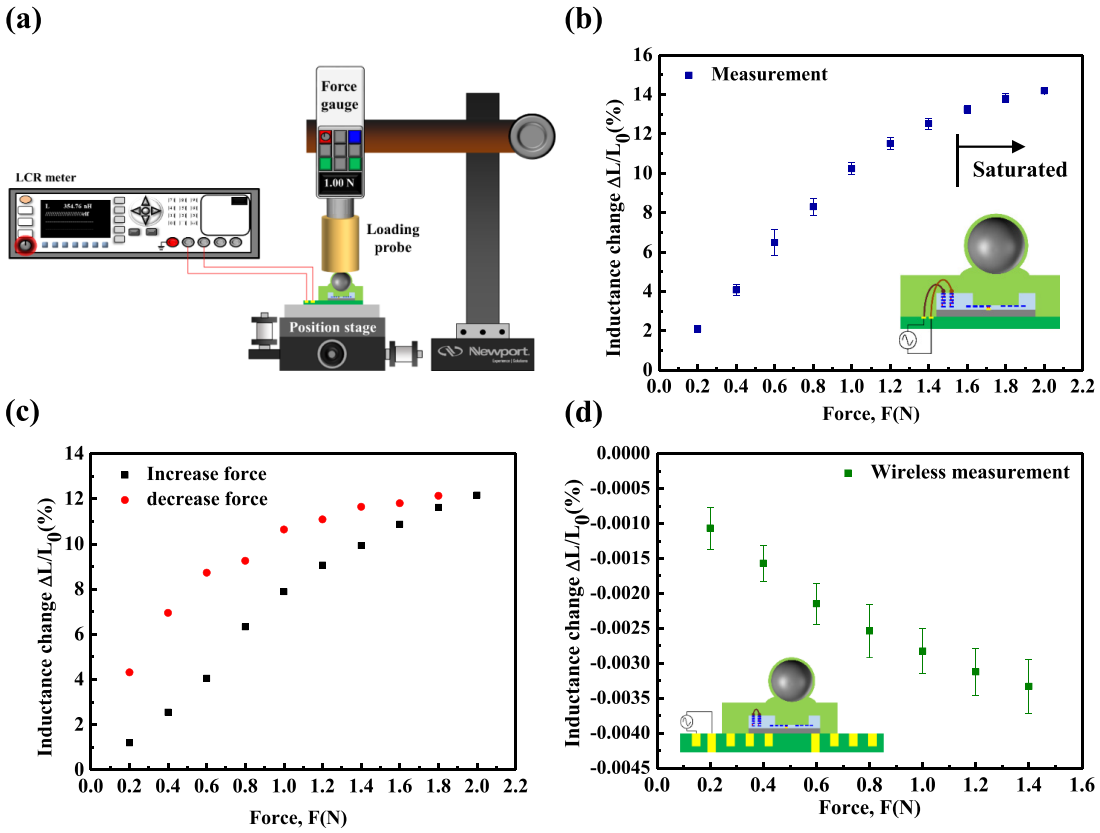

Figure 7. (a) The measurement setup to characterize the performance of tactile sensor, (b) inductance change ($\Delta L/L_0$) versus force measured by the presented tactile sensor, (c) comparison of the signal variation between increase load and decrease load due to the hysteresis effect of polymer, and (d) the force response measured by the reading coil on PCB using the passive wireless sensing approach.

to the cavity depth h on the CMOS chip (near 10 μm), the acrylic mold could offer the polymer an additional thickness of H (near 150–320 μm in this study). Thus, the force sensing range and sensitivity of the tactile sensor could be modulated by varying the thickness H. After curing and demolding of the polymer, an additional polymer was dispensed by the pneumatic system as the adhesive layer for the chrome steel ball, as depicted in figure 5(f). As shown in figure 5(g), the chrome steel ball was placed onto the polymer encapsulated chip with the assistance of a vacuum head and position stages. Finally, as illustrated in figure 5(h), the polymer was dispensed on the chrome steel ball to fully cover its surface. Thus, the chrome steel ball was fixed to the polymer-encapsulated sensing chip after polymer curing.

The micrograph in figure 6(a) presents a bird's eye view of the CMOS sensing chip after etching of the sacrificial layers (figure 5(b)). The planar spiral sensing coil (marked by a dashed line) and other test structures were observed. The micrograph in figure 6(b) displays a bird's eye view of the proposed inductive type tactile sensor after the process shown in figure 5(h). The chrome steel ball on top of the CMOS sensing chip is clearly observed. The micrograph in figure 6(c) presents the sensing device on top of a PCB with a reading coil for the use of wireless measurements. The top view of the optical microscope image in figure 6(d) shows the dimension of the sensing coil is 500 μm ($d_{out} = 500$ μm), and the coil with a number of turns of 20 ($N = 20$) was achieved by using the CMOS process. Figure 6(e) indicates the photo of the PCB reading coil. The micrograph and the zoomed in inset in figure 6(f) display the commercially available chrome steel balls with a diameter of 500 μm. The 500 μm diameter chrome steel ball was selected as the force interface since its size was near the minimum spatial resolution of the human finger [21]. The dimensions of the spiral sensing coil ($d_{out} = 500$ μm) was also designed to match the size of the chrome steel ball.

4. Results and discussions

To evaluate the performances and characteristics of the presented sensors, various experiments have been performed in this study. In the following results and discussions, the sensing performance of the sensor, the influence of the fabrication issues, and other characteristics of the sensor are reported.

4.1. Sensing performance of the sensor

The measurement setup in figure 7(a) was established to characterize the performances of the fabricated tactile sensors. The device under test (DUT) was fixed on the micro position stage to control its position in the z-axis. A commercial force gauge with a resolution of 10 mN and capacity of 50 N was used to apply a load on the steel ball of the DUT through a probe, and then the tactile force on sensor was recorded. The force gauge was supported by a fixed mount. After specifying a displacement on the DUT (in the z-axis) by the position

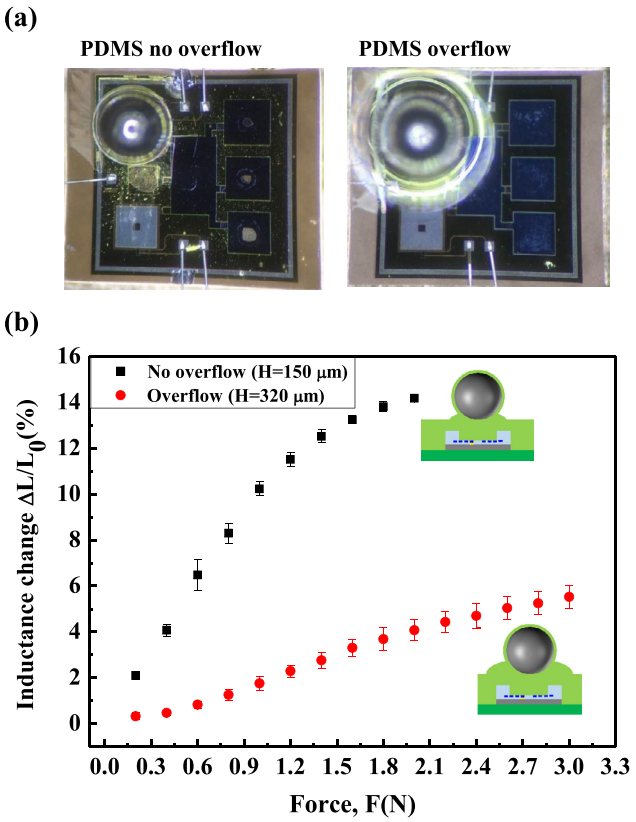

Figure 8. Influence of the polymer thickness H during molding process and polymer dispensing during the chrome steel ball assembly, (a) top view of the devices with different polymer thickness H and volume of dispensed polymer on chrome steel ball, and (b) measurement results to show the performance variation for presented sensors with different polymer thickness H and volume of dispensed polymer on chrome steel ball.

stage, a corresponding force was applied on the tactile sensor. The commercial LCR-meter (Agilent, 4980A) applied an AC signal to the sensing coil of the tactile senor (a peak–peak current of $I_{p-p} = 20$mA was used in this study), and also measured the inductance of the sensing coil. Thus, the inductance change ($\Delta L/L_0$, in %), which varied with tactile forces (F, in Newton) were measured, as shown in figure 7(b). The presented sensor (CMOS chip encapsulated with the 184-PDMS polymer of $H = 150$ μm) had a sensitivity of 9.22 (%/N) and a non-linearity of 2% within the sensing range of 0–1.4 N. The sensing range was defined as 0–1.4 N since the variation of inductance change with force decreased significantly as the tactile load exceeded 1.4 N. The sensitivity had nearly a 5-fold difference, compared to the FEM simulation in figure 4(c). The difference could be a result of the variation in geometry, material properties, etc between the FEM model and real sample. Measurements in figure 7(c) show the results detected during the loading and un-loading tests, and the hysteresis phenomenon due to the polymer layer [22] was observed. Note that no failure occurred on the polymer layer within the loading range (0–2 N) in this study. Measurements in figure 7(d) further demonstrate the capability of wireless sensing for the presented tactile sensor. In this test, the AC signal (also a peak–peak current of $I_{p-p} = 20$ mA) from the LCR meter was introduced to the reading coil on a PCB, and the sensing unit was a passive component. Typical measurement results depict that the inductance of the reading coil decreased as the normal force increased. The wireless sensing sensitivity and non-linearity of the sensor were −0.0018(%/N) and 7(%) within the range of 0–1.4 N, respectively. The trend agrees with the prediction from equation (3), which indicates the decrease of net inductance on the reading coil by the mutual inductance of two coils ($-M \times dI_s/dt$).

4.2. Discussion of the influence of polymer molding and chrome steel ball assembly

As discussed in section 3, the polymer volume will influence the stiffness as well as the sensitivity of the tactile sensor. Moreover, the alignment of the chrome steel ball with the sensing coil will influence the read out signal and further change the sensitivity of the tactile sensor. The samples were prepared to quantitatively evaluate the influence of these two effects during the processes shown in figures 5(e)–(h). Firstly, the samples with different thickness H (the process in figure 5(e)) and different volume of polymer dispensed on the chrome steel ball (the process in figures 5(f)–(h)) were prepared. The micrographs in figure 8(a) show two samples prepared for the tests. The left sample is the same one used for the tests in figure 7(b) with $H = 150$ μm, and the right sample had a thickness of $H = 320$ μm. Moreover, the volume of dispensed polymer (the process in figure 5(h)) for the right sample was higher. Measurements in figure 8(b) show that the sample with a larger polymer thickness (i.e. the right sample in figure 8(a)) had lower sensitivity. This agrees with the trend predicted from the simulation in figure 4(c). In other words, the thickness variation due to the polymer molding and dispensing led to the performance change of the proposed sensor. Secondly, the tests to evaluate the influence of the misaligned chrome steel ball (the process in figure 5(g)) were performed, as shown in figure 9(a). In the tests, the sample with only the CMOS sensing chip encapsulated by the polymer was prepared, and the chrome steel ball was fixed to the loading probe. Thus, the loading position of the chrome steel ball on the sensing chip could be controlled well by using the position stage. This study characterized the sensing signals at the conditions of properly aligned, slightly shifted, and badly misaligned, and the measurement results are presented in figure 9(b). The results indicate that the sensing signals decreased as the ball shifted, and no sensing signals were detected if the ball was badly misaligned. Moreover, better polymer thickness control processes for molding and ball assembly were also required to reduce the performance variation of the sensors.

4.3. Discussion of the influence of polymer stiffness

As indicated in figure 2(c), the variation of the sensing signal (inductance change) with the tactile load for the presented sensor was determined by the following two mechanisms: (1) the polymer deformation (i.e. the ball displacement) caused by the tactile load, and (2) the inductance change caused by

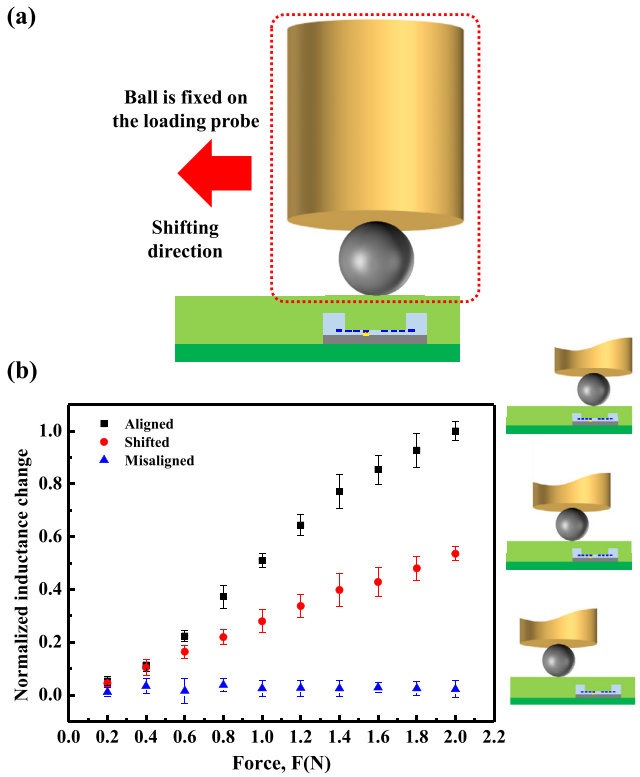

Figure 9. Influence of the alignment issue during the chrome steel ball assembly, (a) schematic view of the misalignment test setup, and (b) force response measurement results to show the influence of the misaligned chrome steel ball.

the ball displacement. According to the proximity sensors reported in [14, 15], the variation of inductance change with the distance of sensing object has poor linearity. To further investigate the influence of the polymer material on the performance of the presented sensor, this study also prepared the CMOS sensing chip encapsulated with a 240 μm thick 527-PDMS. The elastic modulus of 527-PDMS is nearly one order of magnitude smaller than that of the 184-PDMS [8, 23, 24]. The measurements indicate that the compressive elastic modulus of 184-PDMS was near 13-fold higher than that of the 527-PDMS in this study. Moreover, the simulations showed that the sensitivity will decrease near 2-fold as the polymer thickness H increased from 150 μm (for 184-PDMS layer) to 240 μm (for 527-PDMS layer). As a result, the sensitivity of the sensor will increase 6.5-fold when replacing the 150 μm thick 184-PDMS by the 240 μm thick 527-PDMS. Measurements in figure 10(a) depict the inductance change ($\Delta L/L_0$, in %) of the device encapsulated by 527-PDMS at a loading range of 0–0.22 N. Figure 10(b) further shows the comparison of the measurement results in figures 7(b) and 10(a) (sensing chips encapsulated by 184-PDMS and 527-PDMS, respectively). The sensor with a softer polymer (thick 527-PDMS) had a smaller sensing range (0–0.2 N) but higher sensitivity, whereas the device with a stiffer polymer (thin 184-PDMS) could sustain a larger force (0–1.4 N) yet it had lower sensitivity. Within the sensing range, the sensitivity of the sample with 240 μm thick 527-PDMS was 7.5-fold higher than that of the 150 μm 184-PDMS. The result agrees well with the prediction of 6.5-fold. Moreover, the sensing chip with soft

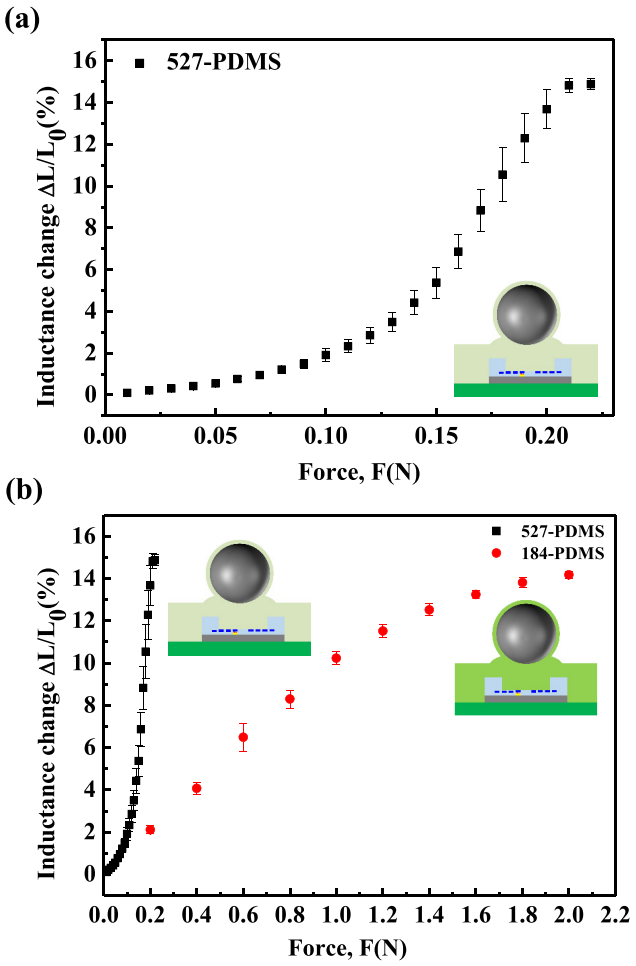

Figure 10. Influence of the polymer stiffness, (a) force response of the sensing chip encapsulated by the 527-PDMS, (b) force response comparison between the sensing chips respectively encapsulated by 184-PDMS (150 μm) and 527-PDMS (240 μm).

527-PDMS had poor linearity for the variation of inductance change with tactile force, and the one with stiff 184-PDMS had good linearity. The good linearity of the sensing chip with the stiff 184-PDMS may contribute from the net effect of the non-linear load-deflection relation of the polymer and the non-linear inductance change with ball displacement. Thus, in addition to the polymer thickness, the selection of polymer materials is critical for the presented sensor.

4.4. Discussion of the influence of contact materials and temperature variation

This study further established the test setups to evaluate the influences of contact materials and temperature for the presented tactile sensors. The electromagnetic type tactile sensor has the problem of sensing signal drift when the contact material is different [12]. Thus the influence of contact materials on the sensing signals of the presented sensor is characterized. As shown in figure 11(a), the probe of three different contact materials including acrylic, aluminum, and stainless steel, were employed to contact and apply load onto the chrome steel ball to characterize the inductance change versus tactile load. The measurement results in figure 11(b) indicate that

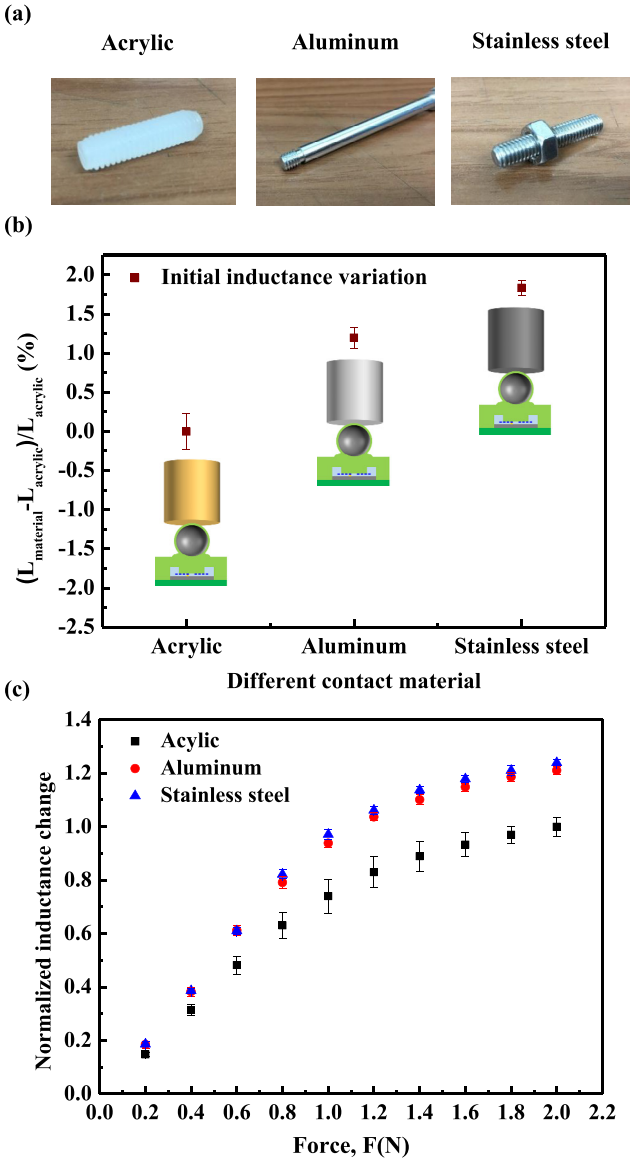

Figure 11. Influence of the contact materials, (a) photos of three different contact materials, (b) offset of the initial inductance as compared with the acrylic probe, and (c) the force response measured using different contact materials.

the initial inductances (without a tactile load) of aluminum and stainless steel probes were 1.2% and 1.8% higher than the acrylic one, respectively. The measurements in figure 11(c) show the variation of inductance change with the tactile load for the three different probes. Note that the nonconductive material will not affect the inductance signal as reported in [15]. Hence, only the conductive materials caused signal variation of the inductive sensors. The normalized inductance changes of the sensor with respect to the acrylic probe are presented in figure 11(c), and the sensitivity of aluminum and stainless steel probes were 1.25-fold and 1.29-fold higher than the acrylic one, respectively, within a sensing range of 0–1.4 N. Thus, calibration of the presented inductive sensors with respect to contact materials was required.

The polymer material has the concern of a large thermal expansion coefficient. Thus, the sensor performances were characterized at four different temperatures including room

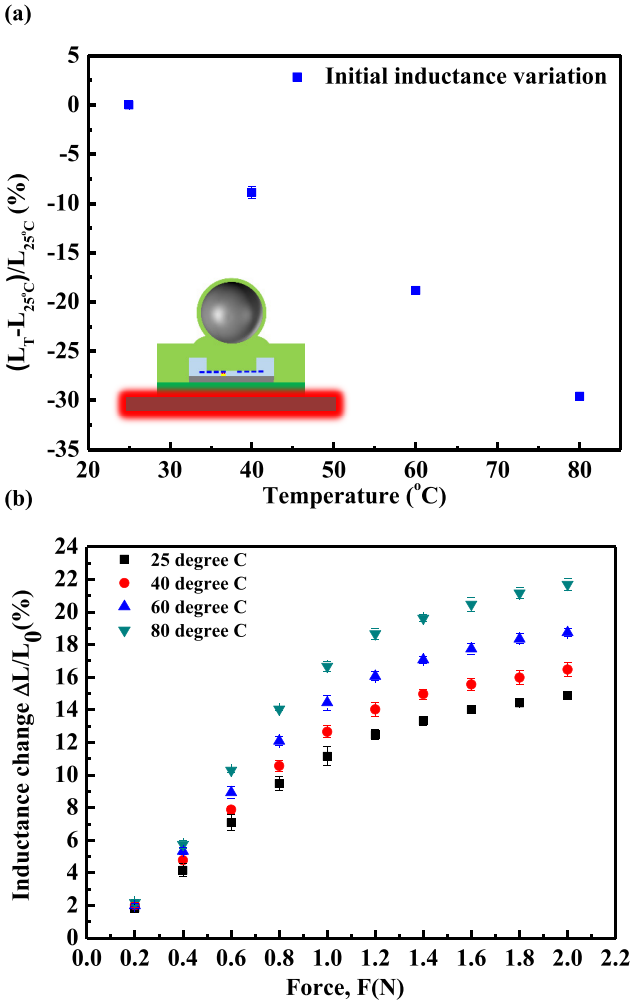

Figure 12. Influence of ambient temperature, (a) initial offset of the tactile sensor at different ambient temperatures, and (b) the inductance change measured at different ambient temperature.

Table 1. The specifications of the proposed CMOS MEMS inductive tactile sensor.

Items	Proposed tactile sensor	Unit
Size of sensing coil	500	μm
Sensing range	0–1.4	N
Sensitivity	9.22	%/N
Nonlinearity	2	%
Span	14.2	%
Repeatability	±0.7 (Max)	%
Temperature coefficient of offset	−0.53	%/°C
Temperature coefficient of sensitivity	0.98	%/°C

temperature (25 °C), 40 °C, 60 °C, and 80 °C. In this experiment, the microscope heating stage was used to specify the temperature for the loading tests. The measurements in figure 12(a) show the initial offset of the inductance without tactile load ($(L_T - L_{room})/L_{room}$, in %) at different temperatures (L_T: inductance at different temperature, L_{room}: inductance at room temperature), and the TCO (temperature coefficient of offset) of the sensor was determined as −0.53(%/°C). As the ambient temperature elevated, the

polymer expanded to increase the distance between the chrome steel ball and the sensing coil, so that the inductance of the sensing coil decreased. The sensitivity (variation of inductance change with tactile force, $(\Delta L/L_0)/F$) of the presented tactile sensor at different temperatures was also characterized, as shown in figure 12(b). This indicates the sensitivity of the sensor at 80 °C was 1.54-fold higher than that at 25 °C within a sensing range of 0–1.4 N. Hence, the presented sensor had a TCS (temperature coefficient of sensitivity) of 0.98(%/°C). The increase of sensitivity ($(\Delta L/L_0)/F$) at an ambient temperature contributed from the decrease of initial inductance depicted in figure 12(a). Finally, table 1 summarizes the specification of the proposed CMOS MEMS inductive type tactile sensor.

5. Conclusions

In this work, a CMOS MEMS inductive type tactile sensor integrated with a chrome steel ball sensing interface was designed and implemented using the TSMC 0.18 μm 1P6M CMOS process and the in-house polymer packaging approach. We take the advantages of (1) the existing foundry service to provide mature CMOS fabrication technologies, and (2) the CMOS process with multi layers stacking, for the sensing chip design. The proposed design employed a polymer to act as the deformable spring, hence no fragile suspended thin film structures were required. Thus, unwanted deformations due to residual stresses and CTE mismatch of suspended thin films for the CMOS chip were prevented. This work has implemented the presented sensors and also characterized their performance; sensitivity within a sensing range of 0–1.4 N was 9.22(%/N). Passive wireless sensing using the PCB reading coil was also demonstrated. Issues influencing the performance of the presented sensors were also investigated, including the assembly of the chrome steel ball, polymer stiffness, contact materials, and ambient temperature. The misalignment of the chrome steel ball reduced the sensitivity of the presented sensor. The presented device has the potential to modulate performances such as the sensitivity and sensing range by changing the encapsulated polymer. However, the very different load-deflection relationship between polymers is a concern and further investigations are required. Moreover, better polymer thickness control processes for molding and ball assembly are also required to reduce the performance variation of the sensors. The conductive contact object will influence the magnetic flux and further cause the signal variation of the presented inductive sensors. Thus, the sensitivity of aluminum and stainless steel probes are higher than the acrylic probe within a sensing range of 0–1.4 N. The measurements also show that the thermal influence by ambient temperature variation for the presented sensor at the TCO of initial inductance was −0.53(%/°C), and the TCS was 0.98(%/°C). Table 1 summarizes the specification of the proposed CMOS MEMS inductive type tactile sensor. Note that the material properties such as hysteresis, durability, etc. for the polymer are important concerns for future applications.

Acknowledgments

This research was sponsored in part by the Ministry of Science and Technology of Taiwan under grants MOST 104-2221-E-007-016-MY3, MOST 105-2221-E-007-026-MY3, and MOST 106-2622-8-007-006-TE3. The authors want to show their appreciation for the TSMC and the National Chip Implementation Center (CIC), Taiwan, for supporting the manufacture of the CMOS chip. The authors would also like to thank the National Center for High-Performance Computing (NCHC) for support of simulation tools, and Dr Jiunn-Horng Lee of NCHC for his valuable help with the simulation. The authors also would like to show their appreciation for the Center for Nanotechnology, Materials Science and Microsystems (CNMM) of National Tsing Hua University and the National Nano Device Laboratory (NDL), Taiwan for providing the process tool.

ORCID iDs

Weileun Fang https://orcid.org/0000-0002-6000-026X

References

[1] Vásárhelyi G, Ádám M, Vázsonyi É, Vízváry Z, Kis A, Bársony I and Dücsõ C 2006 Characterization of an integrable single-crystalline 3D tactile sensor *IEEE Sens. J.* **6** 928–34
[2] Hwang E-S, Seo J-h and Kim Y-J 2007 A polymer-based flexible tactile sensor for both normal and shear load detections and its application for robotics *J. Microelectromech. Syst.* **16** 556–63
[3] Kim J-H, Choi W-C, Kwon H-J and Kang D-I 2006 Development of tactile sensor with functions of contact force and thermal sensing for attachment to intelligent robot finger tip *IEEE Sensors (Daegu, Korea)* pp 1468–72
[4] Nguyen T-V, Nguyen B-K, Takahashi H, Matsumoto K and Shimoyama I 2014 High-sensitivity triaxial tactile sensor with elastic microstructures pressing on piezoresistive cantilevers *Sensors Actuators* A **215** 167–75
[5] Ádám M, Mohácsy T, Jónás P, Dücso C, Vázsonyi E and Bársony I 2008 CMOS integrated tactile sensor array by porous Si bulk micromachining *Sensors Actuators* A **142** 192–5
[6] Takahashi H, Nakaia A, Thanh-Vinh N, Matsumoto K and Shimoyama I 2013 A triaxial tactile sensor without crosstalk using pairs of piezoresistive beams with sidewall doping *Sensors Actuators* A **199** 43–8
[7] Wen C-C and Fang W 2008 Tuning the sensing range and sensitivity of three axes tactile sensors using the polymer composite membrane *Sensors Actuators* A **145** 14–22
[8] Liu Y-C, Sun C-M, Lin L-Y, Tsai M-H and Fang W 2011 Development of a CMOS-based capacitive tactile sensor with adjustable sensing range and sensitivity using polymer fill-in *J. Microelectromech. Syst.* **20** 119–27
[9] Lai W-C and Fang W 2015 Novel two-stage CMOS-MEMS capacitive-type tactile-sensor with ER-fluid fill-in for sensitivity and sensing range enhancement *Transducers (Anchorage, Alaska)* pp 1175–8
[10] Yeh S-K, Chang H-C and Fang W 2017 A novel polymer filled CMOS-MEMS inductive-type tactile sensor with wireless sensing capability *Transducers (Kaohsiung, Taiwan)* pp 834–7

[11] Amor A-B, Budde T and Gatzen H-H 2006 A magnetoelastic microtransformer-based microstrain gauge *Sensors Actuators* A **129** 41–4
[12] Wattanasarn S, Noda K, Matsumoto K and Shimoyama I 2012 3D flexible tactile sensor using electromagnetic induction coils *IEEE MEMS (Paris, France)* pp 488–91
[13] Chang H-C *et al* 2014 Magnetostrictive type tactile sensor based on metal embedded polymer architecture *IEEE MEMS (San Francisco, CA)* pp 1189–92
[14] Lo P-H, Hong C, La S-C and Fang W 2011 Implementation of inductive proximity sensor using nanoporous anodic aluminum oxide layer *Transducers (Beijing, China)* pp 1871–4
[15] Lo P-H, Tseng S-H, Yeh J-H and Fang W 2013 Development of a proximity sensor with vertically monolithic integrated inductive and capacitive sensing units *J. Micromech. Microeng.* **23** 035013
[16] Cheng C-L, Tsai M-H and Fang W 2015 Determining the thermal expansion coefficient of thin films for a CMOS MEMS process using test cantilevers *J. Micromech. Microeng.* **25** 025014
[17] Musunuri S, Chapman P L, Zou J and Liu C 2005 Design issues for monolithic DC–DC converters *IEEE Trans. Power Electron.* **20** 639–49
[18] Mohan S S, Hershenson M M, Boyd S P and Lee T H 1999 Simple accurate expressions for planar spiral inductances *IEEE J. Solid-State Circuits* **34** 1419–24
[19] Finkenzeller K 2010 *RFID Handbook: Fundamentals and Applications in Contactless Smart Cards, Radio Frequency Identification and Near-Field Communication* (New York: Wiley)
[20] Tsai M-H, Sun C-M, Liu Y-C, Wang C and Fang W 2009 Design and application of a metal wet-etching post-process for the improvement of CMOS-MEMS capacitive sensors *J. Micromech. Microeng.* **19** 105017
[21] Dahiya R S and Valle M 2012 *Robotic Tactile Sensing: Technologies and System* (Berlin: Springer)
[22] Kim T K, Kim J K and Jeong O C 2011 Measurement of nonlinear mechanical properties of PDMS elastomer *Microelectron. Eng.* **88** 1982–5
[23] Schneider F, Fellner T, Wilde J and Wallrabe U 2008 Mechanical properties of silicones for MEMS *J. Micromech. Microeng.* **18** 065008
[24] Johnston I D, McCluskey D K, Tan C K L and Tracey M C 2014 Mechanical characterization of bulk Sylgard 184 for microfluidics and microengineering *J. Micromech. Microeng.* **24** 035017